Brain Research 1644 (2016) 267–277

Contents lists available at ScienceDirect

Brain Research

journal homepage: www.elsevier.com/locate/brainres

Research report

Focal attenuation of specific electroencephalographic power over the right parahippocampal region during transcerebral copper screening in living subjects and hemispheric asymmetric voltages in fixed brain tissue

Nicolas Rouleau [a], Brendan Lehman [b], Michael A. Persinger [a,*]

[a] Biomolecular Sciences & Behavioural Neuroscience Programs, Laurentian University, 935 Ramsey Lake Road, Sudbury, Ontario, Canada P3E 2C6
[b] Department of Biology & Behavioural Neuroscience Program, Laurentian University, 935 Ramsey Lake Road, Sudbury, Ontario, Canada P3E 2C6

ARTICLE INFO

Article history:
Received 10 June 2015
Received in revised form
17 December 2015
Accepted 17 May 2016
Available online 19 May 2016

Keywords:
QEEG
LORETA
Parahippocampal gyrus
Entorhinal cortices
Human brain
Theta activity

ABSTRACT

Covering the heads of human volunteers with a toque lined with copper mesh compared to no mesh resulted in significant diminishments in quantitative electroencephalographic power within theta and beta-gamma bands over the right caudal hemisphere. The effect was most evident in women compared to men. The significant attenuation of power was verified by LORETA (low resolution electromagnetic tomography) within the parahippocampal region of the right hemisphere. Direct measurements of frequency-dependent voltages of coronal section preserved in ethanol-formalin-acetic acid from our human brain collection revealed consistently elevated power ($0.2\ \mu V^2\ Hz^{-1}$) in right hemispheric structures compared to left. The discrepancy was most pronounced in the grey (cortical) matter of the right parahippocampal region. Probing the superficial convexities of the cerebrum in an unsectioned human brain demonstrated rostrocaudal differences in hemispheric spectral power density asymmetries, particularly over caudal and parahippocampal regions, which were altered as a function of the chemical and spatial contexts imposed upon the tissue. These results indicate that the heterogeneous response of the human cerebrum to covering of the head by a thin conductor could reflect an intrinsic structure and unique electrical property of the (entorhinal) cortices of the right caudal hemisphere that persists in fixed tissue.

© 2016 Elsevier B.V. All rights reserved.

1. Introduction

One of the basic assumptions for biological systems and of the human brain as a subset of these systems is that structure dictates function and hence microstructure determines microfunction. As quantitative precision and instruments have evolved over the centuries the presumed homogeneity of structure within the cerebral volume has been modified to accommodate this "complex heterogeneity". For example with the development of flat-mapping and the application of non-linear geometries to the sulcal and gyral patterns, the relative absence of geometric similarity between the left and right hemispheres of the human cerebrum was visualized. In 1997 Van Essen and Drury showed that of the ~80 "folding patterns" discernable in both hemispheres only four (pairs): the central sulcus, Sylvian fissure on the lateral side, the calcarine fissure on the medial side and the cingulate sulcus, were in similar locations. The others exhibited asymmetries. For example the posterior inferior temporal sulcus showed a y-shaped pattern in the right hemisphere but a single linearity in the left. With such propensity for structural anisotropy one would expect a geometric-based potential difference (voltage) that is likely to be frequency-dependent.

Quantitative electroencephalograph (qEEG) and the complex algorithms applied to these data have reiterated the heterogeneity of power densities for inferences of potential differences (voltages) measured a few cm over the cerebral surface as well as the time-dependent alterations in those patterns. The slightly larger voltage measures within the alpha frequency (8–13 Hz) range over the caudal right hemisphere compared to other brain regions which were evident in the days of strip-chart recordings (Morgan et al., 1971), has been enhanced and differentiated. The enhancements can occur over larger regions of the cerebral surface. For example the trans-surface microstate analyses described by Lehmann (1990) and developed by Koenig et al. (2002) revealed the remarkable stability of these states, some of which are

* Correspondence to: Departments of Psychology and Biology, Laurentian University, 935 Ramsey Lake Road, Sudbury, Ontario, Canada P3E 2C6.
E-mail address: mpersinger@laurentian.ca (M.A. Persinger).

http://dx.doi.org/10.1016/j.brainres.2016.05.034
0006-8993/© 2016 Elsevier B.V. All rights reserved.

hemispherically asymmetric or "diagonally connected", over people"s lifetimes. Inferences of three dimensional dynamic structure, as inferred by LORETA (low resolution electromagnetic tomography), have allowed discernment of intrinsic differences in regional displays of current density coupled to specific frequency bands.

Although there has been substantial documentation concerning the quantitative properties of cerebral structure and function during rest states or those associated with cognitive challenges, the response of cerebral activity to proximal physical boundaries such as conductors has been less frequently pursued. However metallic helmets and other containments for the human head could potentially affect not only measurements but cerebral function. Here we present evidence that when normal people wear a head-covering lined with copper mesh compared to the same covering without copper mesh, a local attenuation of power within specific frequency bands occurred only over the right caudal area. LORETA analyses indicated the region involved was centralized around and within the right parahippocampal region.

This region is very significant because it contains the entorhinal cortices (Pruessner et al., 2002) which is the primary input to the hippocampal formation whose function is important for the initial stages of representation of experiences or memory (Van Strien et al., 2009; Witter, 1993). The area is known structurally for its multimodal integration of information from and to the entire neocortices and for the unusual stellate cells (the stratum stellar of Stephan) that contains pace-maker neurons that continually generate 8 Hz oscillations with peak-to-peak changes of a few mV (Alonso and Klink, 1993). Interestingly, the energy associated with this increment is remarkably congruent with Landauer"s threshold when 1 bit of information is dissipated to entropy or two operations converge (Saroka and Persinger, 2014). This region is also the area that has been directly correlated or inferred to be associated with weak increases in geomagnetic activity as well as simulations of that activity within the laboratory (Saroka et al., 2014).

In this article we present the results that show electrophysiological activity within the right caudal hemisphere differentially responds to trans-cerebral "shielding". In addition, we found that direct measurements of coronal sections of human brains which had been maintained in ethanol-formalin-acetic acid for decades exhibited visible integrity of general cytological structure within the cerebral cortex revealed a consistent hemispheric anisotropy in potential difference with specific EEG related frequency bands. These increments included potential within the theta (4–7 Hz) band, sufficient to reflect resonance "circuits", within the grey matter (cortices) of the right parahippocampal region. Finally, and in consideration of the intra-cranial environment, we identified rostrocaudal asymmetries in frequency-dependent hemispheric spectral power density as well as spatial-chemical discriminant factors in a whole, unsectioned fixed brain.

2. Results

2.1. qEEG while wearing copper screen-line toque

The presence of plates or surgical metals in some of our patients over the years produced conspicuous changes in strip-chart amplitudes and some frequency modulation over the sites of implant. However the effects of covering the entire scalp with a conductor and then placing more modern sensor caps over the copper lining has not been employed routinely. A priori, one would expect some difference over the right caudal hemisphere in light of the well known enhancement of alpha power over this region.

To test this hypothesis we custom-constructed two cloth coverings shaped like toques. One was lined with 28 gauge copper mesh such that when it was placed on the head the entire brain would be covered. The second identical toque contained no mesh. Following approval by the university's human ethics committee and signed consent a total of twelve men and women from university classes were recruited. Each subject sat within a comfortable arm chair that was housed within an acoustic chamber that was also a Faraday cage (13 m^3). The resultant geomagnetic field within the space was reduced from 45,000 nT to 20,000 nT (Persinger et al., 2015). For the first or second half of the measurements each subject wore the wire lined toque or the control toque. The order was counterbalanced.

A Mitsar 19-channel Quantitative Electroencephalography (qEEG) system connected to a Lenovo ThinkPad laptop running Windows 7 logged electric potential difference from the surface of the scalp referenced to an average of sensors placed on the ears. The qEEG cap contained sensors positioned according to the 10–20 International System of Electrode Placement. A sodium-based electrogel was applied in order to establish a cap-scalp interface. Data were collected for 1 min when the subject"s eyes were closed and for 1 min while the eyes were opened. Data were extracted as spectral power densities and uploaded to SPSS v20. All recording equipment was outside the closed chamber and the only contact with the subject during the recording was through a lapel microphone.

The results were quantitatively evident. Aggregated potentials from the right caudal sensors (T6, P4, and O2) displayed a decrease in global power spectral density ($\mu V^2\,Hz^{-1}$) during the copper-lined condition ($M=5.16$, $SE=1.85$) relative to the control condition ($M=5.98$, $SE=2.08$) when the participants' eyes closed, $t(11)=2.18$, $p=0.05$. This was not measured for other cerebral regions and was not apparent in the right caudal sensors when the participants' eyes were open ($p>0.05$).

To discern a specific frequency-band source for this effect, global power was separated into low frequency (1.5–14 Hz) and high-frequency (14–40 Hz) band ranges. The right caudal sensor cluster displayed a decrease in high-frequency $\mu V^2\,Hz^{-1}$ during the copper-lined condition ($M=1.59$, $SE=0.73$) relative to the control condition ($M=1.91$, $SE=0.81$) when the participants' eyes were closed, $t(11)=2.89$, $p<0.05$. The contralateral sensor cluster (T5, P3, and O1) also demonstrated a comparable decrease of $\sim 0.33\ \mu V^2\,Hz^{-1}$ during the copper-lined condition relative to the control condition when for this band of high-frequencies, $t(11)=2.37$, $p<0.05$.

Inspection of the data revealed a conspicuous gender effect. When the females were removed from the analyses the significant decreases in power spectral densities observed during the copper-lined condition were effectively eliminated. Male subjects did not demonstrate decreases in power as a function of cap type within any sensor or band ($p>0.05$). Average decreases of $0.60\ \mu V^2\,Hz^{-1}$ within the high-frequency bands were observed for females during the copper-lined condition relative to control condition, $t(5)=4.41$, $p<0.01$, $r^2=0.80$. In other words for the female subjects wearing or not wearing the copper toque accommodated 80% of the variance in the power variation within the high frequency band.

In addition a specific decrease in theta power over O2 was noted for females only during the copper-lined condition relative to control condition, $t(5)=2.58$, $p=0.05$. This decrease was equivalent to $\sim 0.80\ \mu V^2\,Hz^{-1}$. To discern if there was a finer increment of frequency, spectral frequencies within the theta band (4–7.5 Hz) for the O2 sensor were split into 0.5 Hz increments. A significant decrease in spectral densities within the 5.5 Hz increment were noted during the copper-lined condition, $t(6)=5.41$, $p<0.005$. The same 5.5 Hz increment was associated with a decrease in spectral densities over T6 during the copper-lined

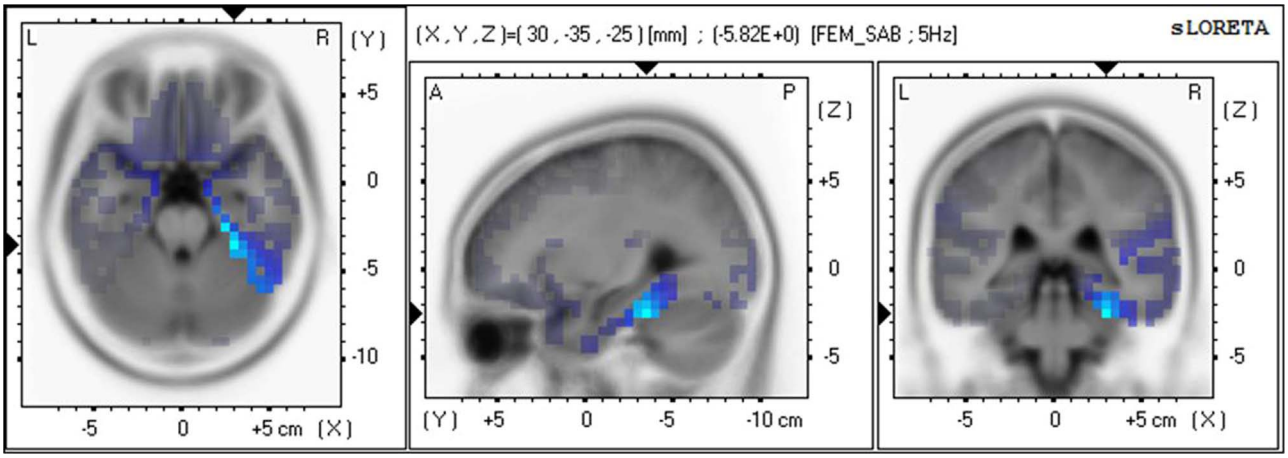

Fig. 1. sLORETA tomogram showing decreased beta2 signals localized to the right fusiform gyrus. MNI coordinates (X, Y, Z): 30, −35, −25.

condition, $t(6)=3.13$, $p<0.05$. In summary a theta power diminishment occurred simply because copper mesh covered the entire skull in a region that is traditionally and frequently associated with indicators of changes in activity within the right parahippocampal region. Consequently we explored source-localization.

2.2. S-LORETA measurements

Standardized low-resolution electromagnetic tomography (sLORETA) was employed as a neuroimaging technique in order to source-localize any potential differences between experimental conditions. Raw data were extracted in 15 s segments from WinEEG, converted to individual cross-spectral files, and further to sLORETA files. Within-subject comparisons were performed with 5000 randomizations and a variance smoothing parameter of 0. Current source densities (CSD) were computed within sLORETA software and uploaded to SPSS v20.

sLORETA source-localized a decrease in beta2 and beta3 power for females only within the right fusiform gryus (Fig. 1) and within the left parahippocampal gyrus (Fig. 2) for the copper-lined condition relative to the control condition. Talairach Client Version 2.4.3 demonstrated the equivalent co-ordinates (X, Y, Z) were −15, −35, 0 corresponding to grey matter of Brodmann area 27. Whereas Brodmann area 27 is classically representative of the presubiculum, the low spatial resolution of sLORETA (~5 mm) would indicate involvement of the adjacent parahippocampal gyrus. Co-ordinates 30, −35, −25 were identified within a cubic range (±4 mm) of right parahippocampal grey matter. The bilateral decreases occurred within the identical position on the Y or rostrocaudal axis (−35). CSD values were extracted for MNI coordinates 30, −35, −25 (right fusiform gyrus) and −15, −35, 0 (left parahippocampal gyrus) from all participants in order to quantify differences as a function of the experimental condition. Descriptive statistics revealed an average CSD value of 5.63 for the control cap condition and a value of 3.90 for the copper-lined cap condition.

2.3. Potential differences from coronal brain sections

The results suggested that there may be something intrinsically unusual about the right parahippocampal region. This region shows unique surface topography that was labeled by Klinger according to Gloor (1997) as “verrucae gyri hippocampi”. They are repeated protrusions along the surface of the rostral component of this region that is primarily entorhinal cortices and are visualized histologically as lozenge-shaped close clusters of cells with relatively cell free intermittent zones within Layer II. The stellate cells in this layer give rise to thick descending axons that form the principal component of the perforant pathway. The structure and connectivity of the entorhinal cortices is considered to be unique and different from any other cortical area.

As a component of the Advanced Human Neuroanatomy Laboratory for the Behavioural Neuroscience Program we have had about 9 human brains maintained in ethanol-formalin-acid acid (EFA) for the last 30 years. Six of these brains were obtained from North Carolina Biological Supply before the moratorium on sale of

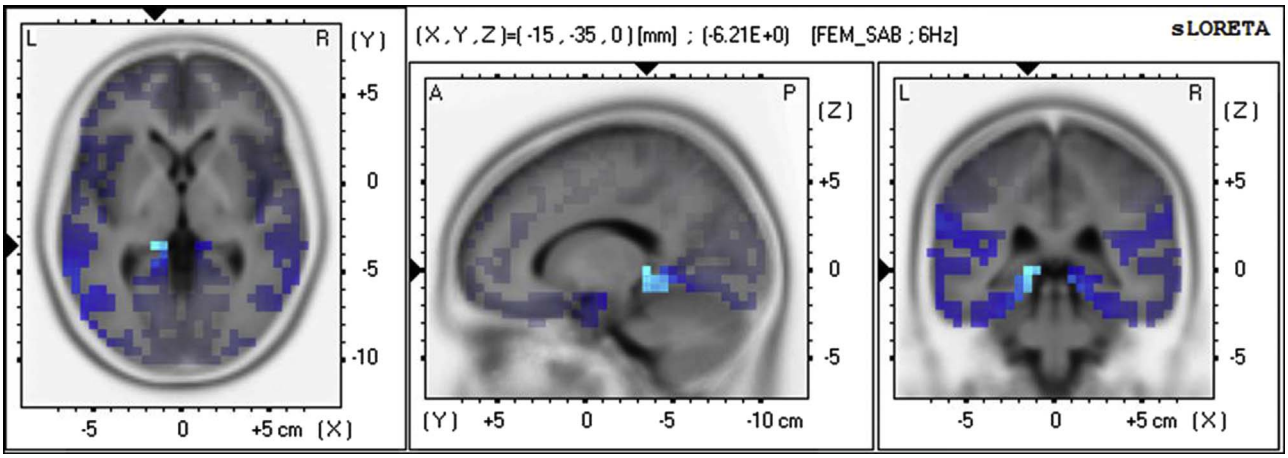

Fig. 2. sLORETA tomogram showing decreased beta3 signals localized to the left parahippocampal gryus. MNI coordinates (X, Y, Z): −15, −35, 0.

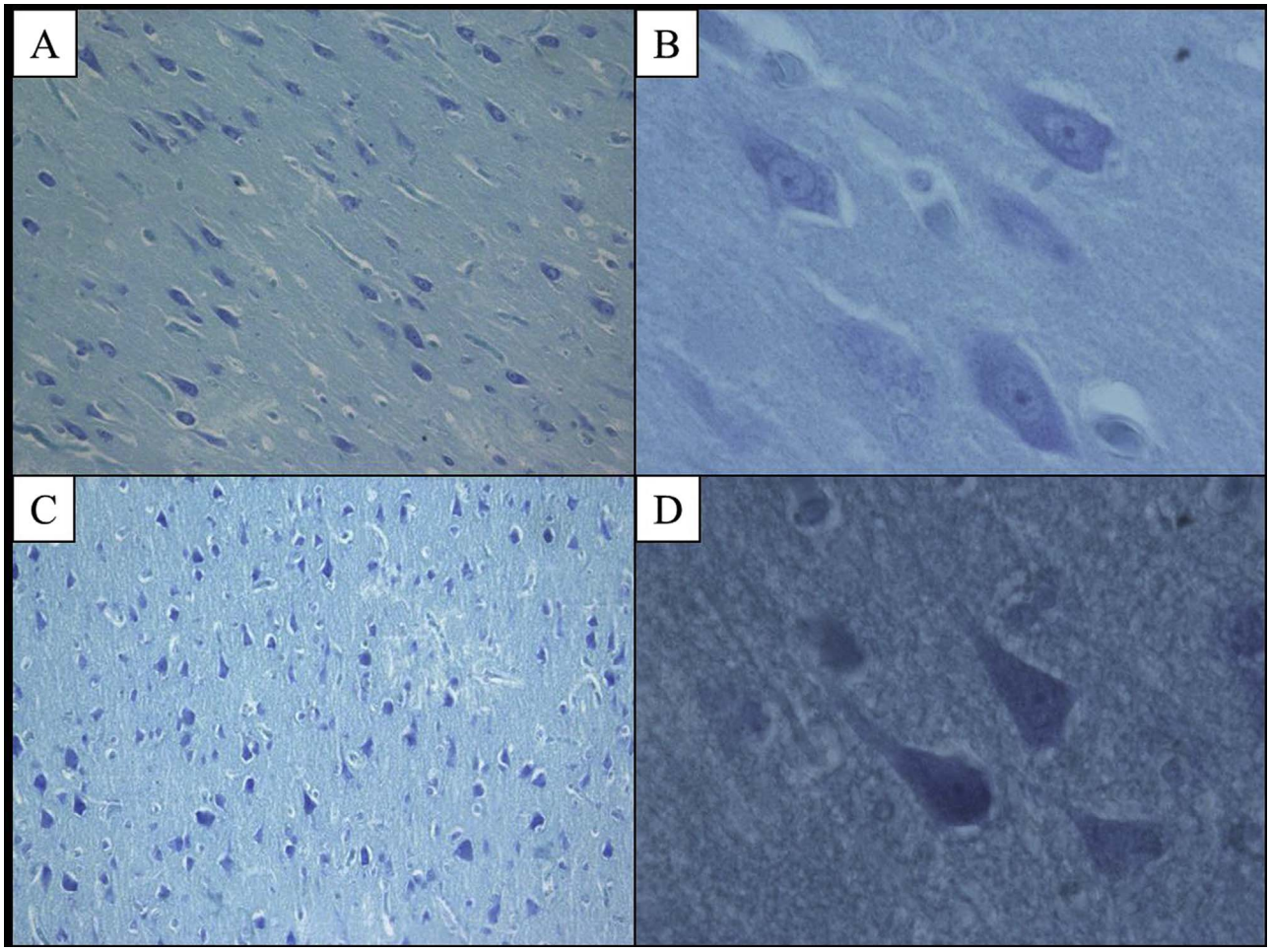

Fig. 3. Cortical section from the frontal cortex at 400 (A) and 1000 (B) times magnification as well as hippocampal grey matter at 400 (C) and 1000 (D) times magnification. These human brains had been fixed in EFA after arrival from the source for more than 25 years before histological processing.

human tissue while another 3 were obtained from anonymous donors. Consequently there was no specific information regarding the genders, the ages (although this can be inferred) or the times of termination of the specimen. Each brain was transferred immediately upon its arrival to its own plastic (Tupperware) container and immersed within EFA where it remained.

EFA stock consists of 75% ethanol, 15% distilled water, 5% formaldehyde, and 5% acetic acid. We have found that EFA is less harsh with the tissue over protracted periods than formalin only. In addition, histological analyses of cortical sections indicate that the cellular structures are in tact even decades later. Fig. 3 illustrates that the integrity of the fixed tissue stored in EFA for sample frontal cortical and hippocampal sections stained with toluidine blue O. Images A and C (400 ×) show preserved polar orientation of the neural parenchyma while images B and D (1000 × oil) reveal a relatively gross preservation of cytomorphology including that of the nucleus with heavy staining of the nucleolus for most cells.

Coronal sections from three of the most intact brains were selected from our collection of human neuroanatomical tissue. It was critical that each slice should contain residual vasculature that remained structurally connected (for qEEG referencing) to the cerebrum. One hundred and six ($n=106$) anatomical features were probed using a single needle-probe. The probe was inserted into the locus of interest referenced to 4 needle-probes coupled to one of the major arterial offshoots of the Circle of Willis where electric potential differences were obtained. Two sections were referenced to the basilar artery and the third was referenced to the middle cerebral artery (MCA). Impedance values from vascular references were regulated to <5 kΩ. Sixty seconds of raw electric potential differences were obtained from each locus of interest. Recordings were classified by type of matter (grey or white), hemisphere (left or right), and longitudinal position (rostral or caudal). All measurements were in the Neurochemistry/Neuroanatomy Laboratory.

The results of the measurements between the left and right hemispheric structures are shown in Table 1. Increased power spectral density equivalent to 0.20 $\mu V^2\ Hz^{-1}$ on average within the gamma band was identified within the right hemisphere ($M=1.31$, $SE=0.10$) relative to the left hemisphere ($M=1.10$, $SE=0.03$), $t(82)=2.01$, $p<0.05$, $r^2=0.05$. Other bands did not demonstrate similar hemispheric disparity ($p>0.05$). Discriminant analysis involving power spectral density within all frequency bands predicting longitudinal position accurately classified 67% of cases in a cross-validated model $\Lambda=0.77$, $\chi^2(1)=18.14$, $p<0.001$, canonical $R^2=0.48$. Increased classification accuracy (69%) was noted if white matter structures were eliminated from the analysis.

Differences in power spectral density associated with all structures between coronal slices were identified within the delta ($p<0.001$) and theta ($p<0.005$) bands. Examining only white matter structures eliminated these differences. Only increases in delta power remained when isolating grey matter structures, $F(2,50)=7.66$, $p=0.001$.

2.4. Left-right parahippocampal gyrus

Three ($n=3$) caudal coronal sections stored in EFA, each

Table 1
Left (L) and Right (R) hemispheric general structure power spectral density ($\mu V^2\,Hz^{-1}$) and voltage (μV).

Band	Spectral power density ($\mu V^2\,Hz^{-1}$)				Voltage (μV)			
	Gen - L (N=44)		Gen - R (N=40)		Gen - L (N=44)		Gen - R (N=40)	
	Mean	SD	Mean	SD	Mean	SD	Mean	SD
Delta	132.11	33.75	131.17	35.40	18.17	9.19	18.11	9.41
Theta	38.55	10.62	38.59	10.68	11.62	6.10	11.62	6.11
Alpha	17.17	3.84	17.91	3.31	10.56	5.00	10.79	4.64
Beta1	4.63	1.80	5.21	2.97	5.27	3.29	5.59	4.22
Beta2	3.06	1.16	3.55	3.08	5.53	3.41	5.96	5.55
Gamma	1.10	0.22	1.31	0.66	3.32	1.48	3.62	2.57
Global	32.77	6.99	32.96	7.50	35.52	16.40	35.62	16.99

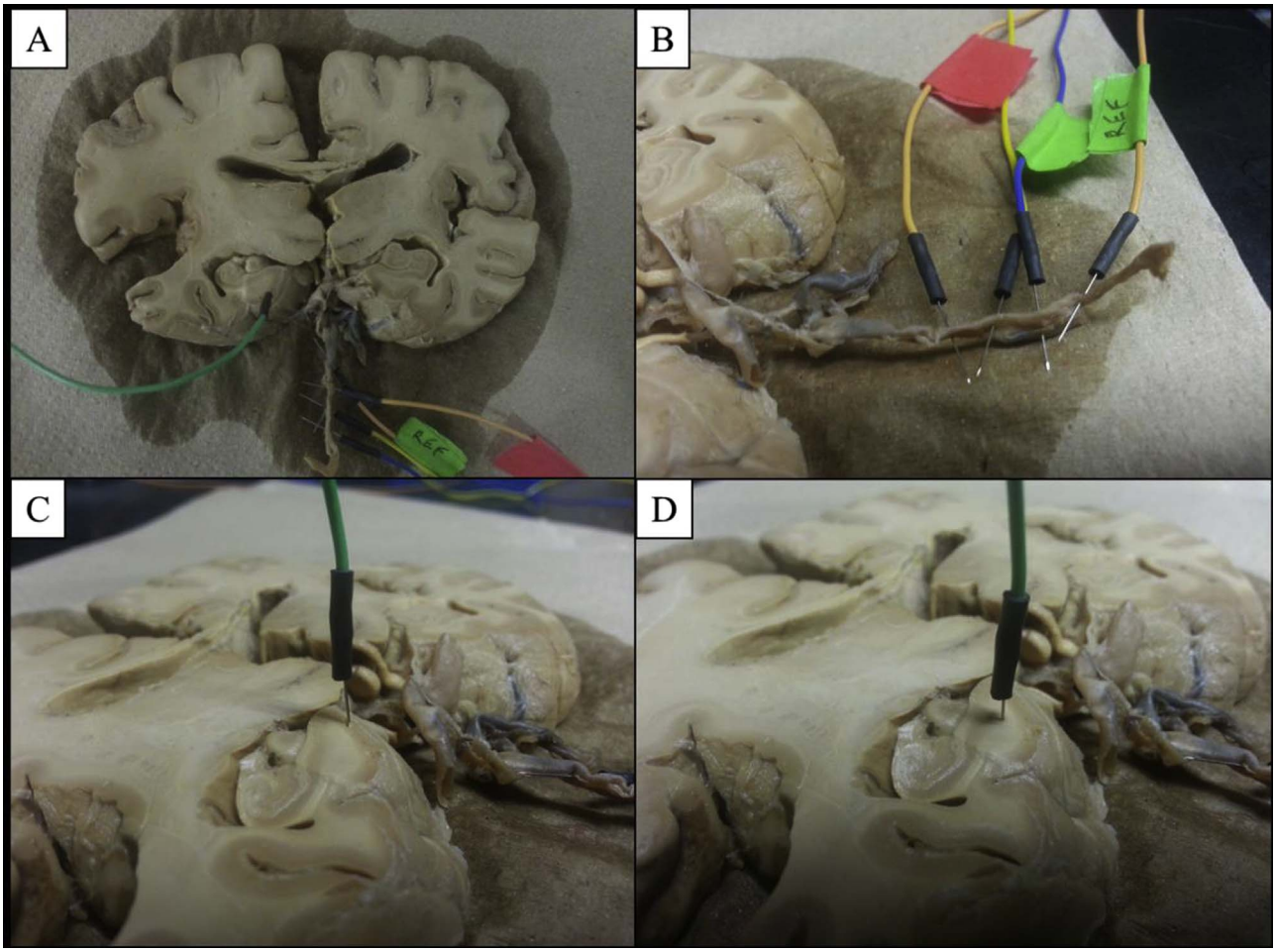

Fig. 4. Experimental setup (A) demonstrating a needle probe inserted into grey (C) and white (D) matter of the parahippocampal gyrus referenced to the basilar artery (B).

derived from a separate brain, containing an intact basilar artery, and clearly defined parahippocampal structures were selected in order to systematically investigate this region of interest. For all practical purposes, the sections were structurally identical in their representation of gross neuroanatomy, angle of the cut, thickness (1–2 cm), and age of preservation. The basilar artery, which served as the electrical reference, was truncated at its caudal end and anchored to the cerebrum by the bilateral remnants of the posterior cerebral arteries (PCA). A total of n=24 recordings were obtained from these sections. Fig. 4 shows the position of needle probes within a coronal slice.

Increased $\mu V^2\,Hz^{-1}$ within the theta band was noted for right parahippocampal grey matter (M=72.06, SE=8.12) relative to left parahippocampal grey matter (M=51.58, SE=4.32), t(10)=2.23, p=0.05, $r^2=0.33$. This increase was equivalent to $\sim 20\,\mu V^2\,Hz^{-1}$ on average. Neither other bands nor parahippocampal white matter displayed this effect ($p > 0.05$). A discriminant analysis involving theta-range power spectral density accurately classified 83% of left-right hemisphere group membership for grey matter only in a cross-validated model $\Lambda=0.67$, $\chi^2(1)=3.82$, p=0.05, canonical $R^2=0.58$.

Differences in theta power associated with parahippocampal structures were identified across coronal slices, F(2,23)=5.24, $p < 0.05$. Power spectral densities within grey matter structures did not differ as a function of coronal slice ($p > 0.05$); however, white matter within the parahippocampal region did demonstrate differences in theta power as a function of coronal section, F(2,11)=10.90, $p < 0.005$.

2.5. Potential differences from an unsectioned brain

The conspicuous rostrocaudal as well as hemispheric differences, which were most evident for the parahippocampal gyri, indicated structure-function anisotropy within the coronal slices. Whereas sectioned tissue samples represent practical sources of investigation, the spatial limits imposed upon the slices represent a degree of separation from the intact organ whose activity is typically measured using qEEG sensors applied over the scalp. Our previous research (Rouleau and Persinger, 2014) that measured a simulated human cerebral cortex composed of dough (flour, salt, water, and citric acid) showed a remarkable concordance of spectral power profiles between the dough when shaped like the human cortices and normal healthy brain activity across the fundamental band (1–40 Hz) when the ambient pH was within a narrow band between 2.47 and 2.52. Slight differences in the concentration resulted in a marked reduction of the coherence with normal EEG activity. The concordance occurred primarily within the higher frequencies (20–40 Hz) and around 8 Hz. Similarly the shape of the dough and its positioning within a skull also facilitated the congruence.

So as to approximate the spatial and chemical contexts within which the brain typically operates, it was necessary to design an experiment in consideration of the intra-cranial environment. To this end, an unsectioned brain which included all telencephalic, diencephalic, and brainstem structures was utilized. The brain was immersed in EFA or distilled H_2O for 20 min prior to measurement. Once removed from the liquid, the brain was placed on a flat surface, within a human replica skull (Fig. 5), or within a polystyrene foam box (Fig. 6). The volume of both "enclosures" was $\sim 0.003\ m^3$. In addition to highlighting the importance of optimal pH, any relevant differences between the spatial conditions could confirm, as Nunez (1995) has previously demonstrated, that the cranial vault is a non-trivial space which contributes to the amplification of specific harmonic frequencies.

Applied to the unsectioned brain were 14 needle-probes inserted into gyri distributed over the surface of the cerebrum. Probes were inserted into the orbiotofrontal (Fp1, Fp2), inferior frontal (F7, F8), parahippocampal (T3, T4), insular (C3, C4), supramarginal (T5, T6), superior parietal (P3, P4), and lateral occipital gyri (O1, O2). Odd numbers referred to probes inserted into the left hemisphere whereas even numbers referred to probes inserted into the right hemisphere. Potential differences between probed loci and reference cup sensors clamped to the ears of $n=2$ human participants were obtained. A sodium-based electrogel was applied to the cup sensors in order to establish an interface with the reference point (i.e. ear lobe), a procedure which is commonplace in qEEG measurement of human participants.

It became apparent that two distinct clusters of sensors could be isolated by dimensional reduction. Spectral power density values for all probes were entered into a factor analysis. A loading coefficient of 0.80 was selected due to the highly redundant signals shared between probes. A rotated component matrix revealed 2 factors, which cumulatively explained 93% of the variance. Probes T3, T4, T5, C3, C4, and P3 loaded on the first factor, explaining 87% of the variance, while Fp1, Fp2, O1 and O2 loaded on the second factor, explaining $\sim$6% of the variance. The first factor consisted of loci which were spatially distributed between the rostral and caudal poles of the cerebrum whereas the second factor consisted of rostral (Fp1, Fp2) and caudal (O1, O2) polar structures. Spectral power densities were averaged across the respective sensor clusters into new variables: Polar and non-polar. Significant differences between these distinct factors as a function of reference sources – the human participants' earlobes – were not noted ($p > 0.05$).

Polar structures were unique in that spectral power densities

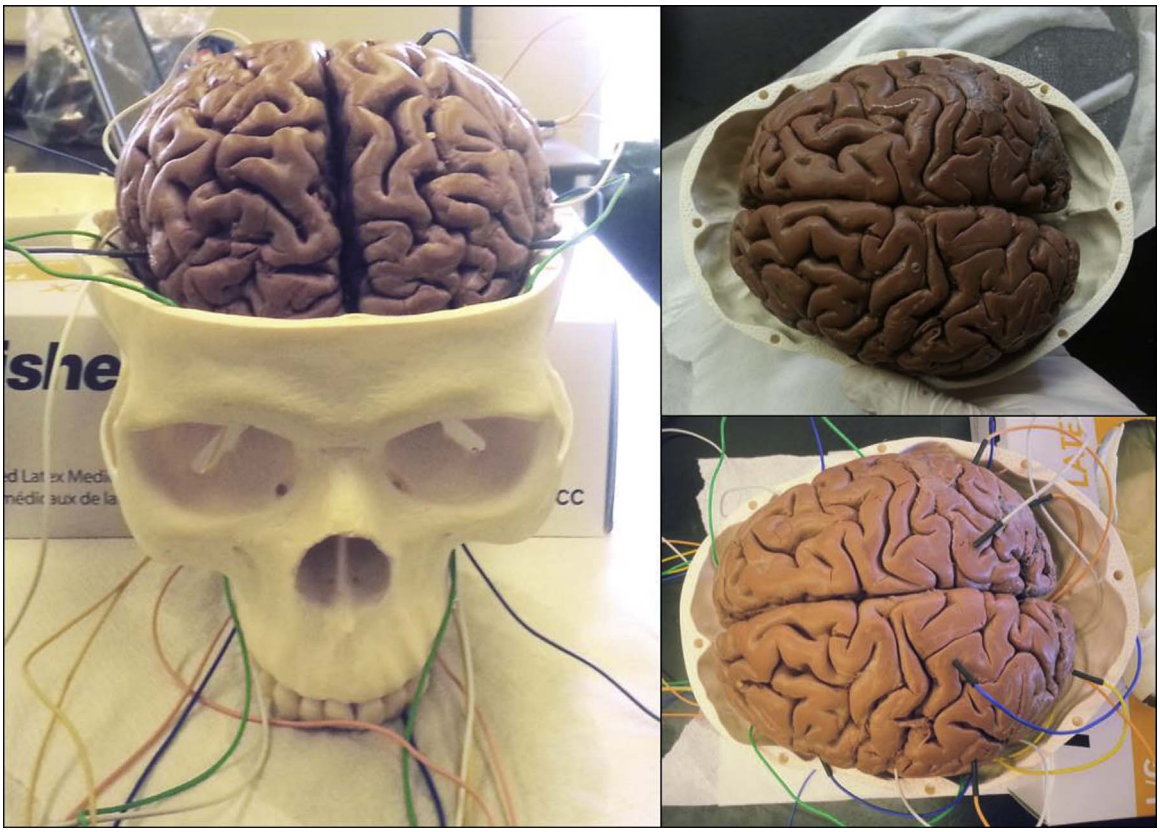

Fig. 5. The brain is equipped with a needle probe array and inserted into the skull. A skull cap (not pictured) encloses the cerebrum within an artificial cranial vault.

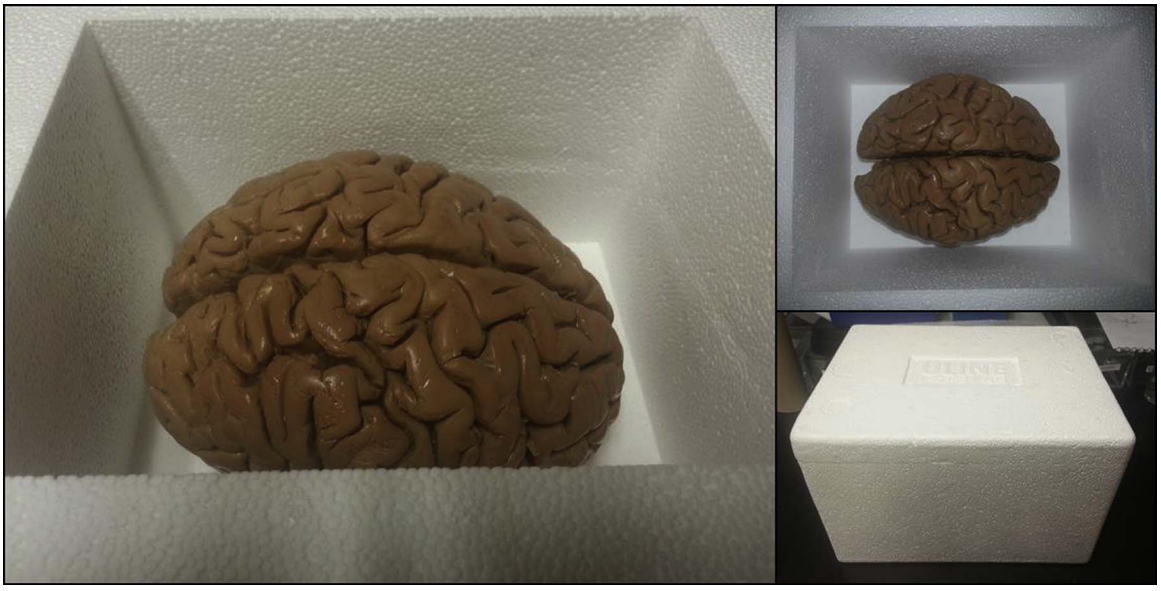

Fig. 6. A polystyrene foam box was employed as a control enclosure within which the brain is placed during recording of electric potential differences.

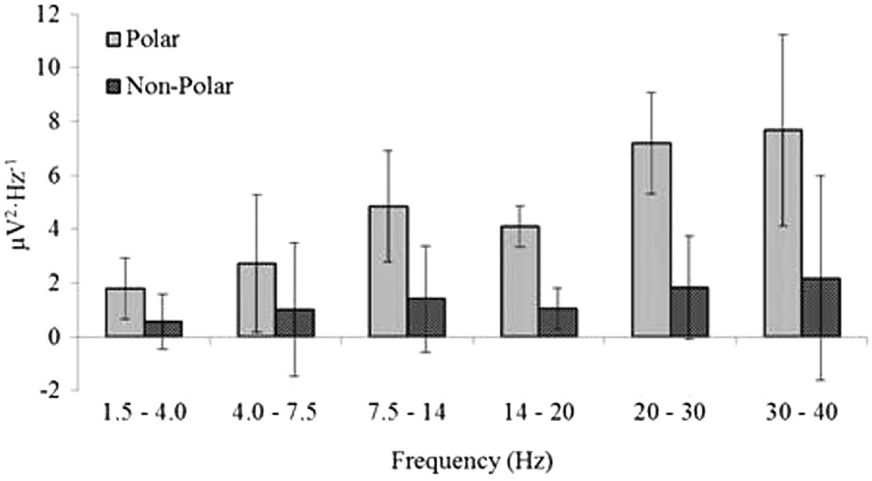

Fig. 7. Power density of polar and non-polar structures as a function of frequency. Means and standard deviations are presented.

obtained from within these convexities varied as a function of the signal frequency, $F(5,143)=27.83$, $p<0.001$, $\eta^2=0.50$. Homogenous subsets isolated common groups using Scheffe's method ($p<0.05$), partitioning the 6 groups into 3 equal increments of frequency which were significantly different: low (1.5–7.5 Hz), middle (7.5–20 Hz), and high (20–40 Hz). Fig. 7 demonstrates these differences. Frequency and polar structure spectral power densities were positively correlated, $r=0.68$, $p<0.001$. Non-polar structures demonstrated an analogous relationship with frequency ($r=0.22$, $p<0.005$); however, a Fisher z-transformation revealed the latter strength of the association was significantly reduced compared to the former, $z=5.08$, $p<0.001$. Spectral power densities within non-polar structures did not differ as a function of frequency ($p>0.05$).

A discriminant analysis accurately classified 60% of cases as a function of whether polar or non-polar structures within the replica human skull were immersed in EFA or H_2O $\Lambda=0.87$, $\chi2(2)=6.05$, $p<0.05$, canonical $R2=0.36$. Discriminant functions were not generated if the brain was placed on a flat surface or within the polystyrene foam box ($p>0.05$). That is, spectral power densities within combined polar and non-polar structures could only be discriminated as a function of the antecedent chemical condition if the brain was placed within a replica human skull. Increased global power within non-polar structures while inside the polystyrene foam box ($M=5.52$, $SE=0.61$) relative to polar structures within the context of the replica skull ($M=4.30$, $SE=0.31$) or the flat surface ($M=4.34$, $SE=0.31$) were noted, $F(2,143)=2.55$, $p=0.01$, $\eta^2=0.06$.

As was the case for coronal sections, rostrocaudal differences were reliably present in the data. Paired *t*-tests examining differences in spectral power density as a function of hemisphere demonstrated conspicuous disparity along the rostrocaudal axis. Orbitofrontal, inferior frontal, and parahippocampal pairs demonstrated increased left hemispheric global power relative to contralateral pairs ($p<0.001$) whereas insular, supramarginal, superior parietal, and lateral occipital pairs demonstrated increased right hemispheric power relative to contralateral pairs ($p<0.001$). Fig. 8 illustrates the left-rostral, right-caudal topography (Table 2).

A conspicuous overlap in left-right spectral densities is noted when the brain is contained within a human replica skull. The parahippocampal (T3-T4) and lateral occipital gyri (O1-O2) show a complete absence of left-right differences in spectral power densities within all frequency bands when contained within the

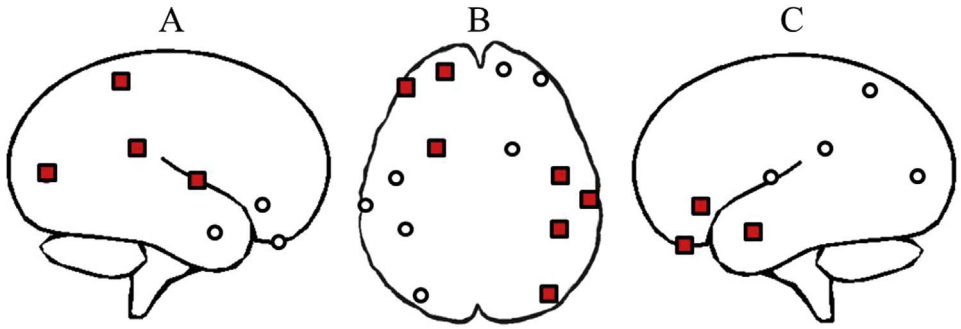

Fig. 8. Right hemispheric (A), dorsal (B), and left hemispheric (C) perspectives of needle-probe (sensor) placement demonstrating rostrocaudal differences in hemispheric spectral power densities where red squares indicate a relative increase compared to the contralateral sensor (circles).

human replica skull ($p > 0.05$). This was not the case for the polystyrene foam box condition or when the brain was placed on a flat surface. An absence of difference in voltage is indicative of increased homogeneity between the sensors. Tables 3 through 5 demonstrate these differences in spectral power density across the sensor pairs as a function of the space of containment.

3. Discussion

The visible heterogeneity of structures between the two human cerebral hemispheres for specific sub-regions, even when accounting for individual differences, has been frequently documented (Good et al., 2001; Raz et al., 2004; Watkins et al., 2001). However, heterogeneity in brain space for electroencephalographic response to a homogenous surface of an applied conductor is less well known. Our measurements of diminished topographical voltages over only the right caudal hemisphere would suggest, at its simplest, either a decrease in current or a decrease in resistivity within this region. Either condition should be associated with a specific pattern or tissue density within this region that is different from most other structures. As a result the properties of the copper mesh (with apertures between 1 and 5 mm, depending upon stretch) specifically diminished the fields emerging from the scalp. Gloor"s (1997) interpretation was that this region is unique because "its structure and connections differ from any other cortical area".

The electroencephalographic region defined by T6, O2, and P4 revealed a specific diminishment of voltage within the 14–40 Hz band when subjects wore the copper mesh toque relative to the toque without lining. In addition the theta power within O2 was also diminished specifically within the 5.5–6 Hz increment within this region and T6. We find this interesting for two reasons. First, one of the most defining neurophysiological features of the hippocampal-entorhinal-trans-cerebral cortical configuration is the powerful theta band upon which a higher "40 Hz" frequency is superimposed (Buzsáki, 2002). The superposition has been considered by many researchers, such as Bear (1996) as evidence of the mechanisms by which initially coded "hippocampal memory" can be distributed throughout the cerebral cortical volume for "long-term" representation. This juxtaposition is also consistent with the supposition that "consciousness" requires a significant "memory" component, that is, the reiterative processing of

Table 3.
Differences in spectral power density between paired-sensors for recordings of the brain placed on a flat surface.

Spectral power density difference ($\mu V^2\ Hz^{-1}$)							
	Fp1-Fp2	F7-F8	T3-T4	C3-C4	T5-T6	P3-P4	O1-O2
Delta	−0.05	0.39	0.01	−0.05	−1.31	−0.48*	−0.04
Theta	0.30*	0.96*	0.09*	−0.12*	−1.12	−0.71*	−0.11
Alpha	0.77*	2.04*	0.26*	−0.18	−5.45	−1.41*	−0.15
Beta1	0.59*	1.85*	0.23*	−0.22*	−2.3	−1.25*	−0.24*
Beta2	1.11*	3.24*	0.43*	−0.3	−2.74*	−2.28*	−0.53*
Gamma	1.14*	3.45*	0.44*	−0.34*	−2.72*	−2.37*	−0.54*

* Indicates significant differences between paired sensors ($p < 0.05$).

Table 4.
Differences in spectral power density between paired-sensors for recordings of the brain placed inside a human replica skull.

Spectral power density difference ($\mu V^2\ Hz^{-1}$)							
	Fp1-Fp2	F7-F8	T3-T4	C3-C4	T5-T6	P3-P4	O1-O2
Delta	0.01	0.46	0	−0.04	−1	−0.46*	0.01
Theta	0.33*	0.99*	0.11	−0.08	−0.80*	−0.68*	−0.11
Alpha	0.31	1.64*	0.06	−0.15	−8.61	−1.20*	0.04
Beta1	0.43	1.67*	0.09	−0.21*	−3.07	−1.16*	−0.13
Beta2	1.07*	3.26*	0.27	−0.33	−3.13	−2.00*	−0.32
Gamma	1.14*	3.33*	0.3	−0.29	−3.14	−2.11*	−0.35

* Indicates significant differences between paired sensors ($p < 0.05$).

Table 2.
Left (L) and Right (R) hemispheric parahippocampal (PHG) grey matter power spectral density ($\mu V^2\ Hz^{-1}$) and voltage (μV).

Band	Spectral power density ($\mu V^2\ Hz^{-1}$)				Voltage (μV)			
	PHG - L (N=12)		PHG - R (N=12)		PHG - L (N=12)		PHG - R (N=12)	
	Mean	SD	Mean	SD	Mean	SD	Mean	SD
Delta	228.05	90.02	273.43	92.16	23.88	15.00	26.15	15.18
Theta	51.58	10.59	72.07	19.90	13.44	6.09	15.88	8.34
Alpha	20.95	4.29	21.07	5.62	11.67	5.28	11.70	6.04
Beta1	6.13	1.71	4.60	1.73	6.06	3.20	5.25	3.22
Beta2	3.17	0.62	3.03	0.90	5.63	2.49	5.50	3.00
Gamma	1.37	0.28	1.15	0.27	3.70	1.67	3.39	1.64
Global	51.88	15.33	62.56	13.69	44.69	24.29	49.08	22.96

Table 5.
Differences in spectral power density between paired-sensors for recordings of the brain placed inside a polystyrene foam box.

Spectral power density difference ($\mu V^2\ Hz^{-1}$)							
	Fp1-Fp2	F7-F8	T3-T4	C3-C4	T5-T6	P3-P4	O1-O2
Delta	0.33*	0.72*	0.09*	−0.13*	−1.44	−0.55*	−0.11*
Theta	0.38*	1.07*	0.12*	−0.17*	−2.46	−0.73*	−0.17*
Alpha	0.70*	1.95*	0.23*	−0.30*	−4.22	−1.45*	−0.30*
Beta1	0.66*	1.91*	0.21*	−0.26*	−2.29	−1.33*	−0.28*
Beta2	1.16*	3.38*	0.35*	−0.47*	−3.22	−2.32*	−0.49*
Gamma	1.12*	3.27*	0.17	−0.67	−2.54*	−2.43*	−0.55*

* Indicates significant differences between paired sensors ($p < 0.05$).

representations of experience within the recursive rostral-caudal electroencephalographic waves coupled to consciousness (Crick and Koch, 1990; Llinas and Ribary, 1993; Meador et al., 2002).

Secondly, “temporal binding” factors in large areas of cerebral activity are considered to be an important condition for consciousness (Crick and Koch, 2003; Joliot et al., 1994). The most frequent candidate is the “40 Hz” band which is reflective of the approximately 20–25 ms recursive rostral-caudal transcerebral fields measured by Llinas and his colleagues many years ago (1991; 1993). While quantifying the derivatives from differences of lagged value, Persinger (1999) calculated that the higher variations that could sequester the 20–25 ms (“40 Hz”) “point durations” of consciousness occurred between 5 Hz and 6 Hz for the lag of a lag condition. For these calculations the actual duration (in ms) of each integer frequency from 1 to 60 Hz was calculated and lagged by one case. The difference between adjacent lags was calculated and lagged. The emergent duration for 20–25 ms was between 5.5 and 6 Hz.

LORETA analyses indicated that the most likely source location for this differential activity when (particularly female) subjects were wearing the toque lined with the copper mesh or not was the right parahippocampal region. Most of the decrease occurred within the higher frequency beta band. These algorithms verified our interpretations that there is some conductive feature within the right ventral caudal hemisphere that is differentially affected (compared to other areas) by the placement of copper mesh over the head.

Differential responsiveness of women's right temporal lobes to the application of burst-firing fields was reported by Richards et al. (1992) who were attempting to discern processes associated with “panics”. The significant interaction between gender and hemisphere of stimulation (left vs right) was due to the marked elevation of reports of fear (e.g., responding affirmatively to post-exposure items such as “I experienced fear or terror” by women who received the right hemispheric stimulation for only 20 min Covariance for clusters of items that are similar to complex partial epileptic signs did not eliminate the interaction suggesting the effect was a direct effect upon structure rather than electrical state.

The other possibility is that this region (as a physiological aggregate), unlike other cerebral cortical areas, responds differentially to the presence of copper mesh. We (Dotta et al., 2014) have shown that cells may respond to reflective features of coverings. Direct measurements of photon emissions (by photomultiplier units) from cancer cells covered by different optical filters (10 nm increments) produced more photon flux density than if there had been no filters. Because the filters are actually micromirrors we concluded that reflection of emitting photons that did not pass through the filter back onto the source stimulated the cells to enhance photon emission. Whether or not cortical cells, the primary source of electroencephalographic power, can respond to the presence of proximal conductors like copper must still be established.

Although our sample was relatively small (6 men, 6 women) the gender effect was conspicuous and suggested a right hemispheric specificity. Good et al. (2001) who employed a voxel-based morphometric analysis of 465 normal adult human brains observed the expected asymmetry of cerebral white and grey matter in the occipital, frontal, and (petalia) temporal lobes as well as the hippocampus. In addition, females displayed increased grey matter with minimal asymmetry in the cortical mantle, parahippocampal gyri, the banks of the calcarine sulci, the cingulate region as well as increased neuronal density and numbers of cells within the temporal cortices. The very specific increase in grey matter within the left parahippocampal gyrus (−15, −34, −4) for females was almost exactly the same coordinates as our MNI values, which also approximates Talairach space, demonstrated for females who wore the copper mesh lined toque.

If our results are coupled to actual structures then they should compliment more traditional morphometric studies. Insausti et al. (1998) who examined MR volumetry from healthy volunteers and autopsy cases indicated significantly large volumes for the entorhinal and perirhinal cortices for the right compared to the left hemisphere. The mean number of 2-mm MR imaging sections for the right and left entorhinal cortices which is most of the parahippocampal gyrus was 11.9 and 11.3, respectively.

The ratio of the difference is about 1.05. If we assume the ranges reported in their data reflected 95% of the population, then the standard deviations would be about 1.5 sections. Consequently hemispheric differences would account for about 8–10% of the variance. During our measurements with volunteers the difference (attenuation of power) over the right caudal hemisphere was about 0.3 $\mu V^2\ Hz^{-1}$ compared to the typical 6 $\mu V^2\ Hz^{-1}$ which is a comparable ratio. This would be consistent with but not a demonstration that the attenuation effect was simply coupled to volume. One possible explanation is the greater the “volume voltage” the greater the current and hence the differential induction by the covering copper mesh that resulted in the attenuated qEEG. However the effect was frequency band-specific which suggests the effect was not a simple d.c. (steady potential) response.

The measurement of a cerebral asymmetry in fixed coronal sections for potential differences between the right and left hemisphere in general and specifically for the parahippocampal region strongly suggests an intrinsic structural feature that is not coupled to living brain or to the metabolic processes such as blood flow. The slightly elevated voltage (0.2 μV) in the right compared to the left hemispheric structures and the conspicuously elevated (2 μV) potential in the right compared to the left parahippocampal grey matter within the theta range in fixed coronal sections suggests there may be relatively resilient structural properties within this region. This greater discrepancy of potential difference in the parahippocampal grey on average compared to general hemispheric asymmetry would be consistent with Insausti et al. (1998) who found a larger volume for the entorhinal cortices in the right hemisphere compared to the left.

Higher intrinsic potential for power densities could contribute to more current density that would allow greater initial voltage potentials from this region. When interacting with the copper mesh the resultant current and magnetic field would potentially attenuate the source. Although surface qEEG is not easily accessible to a ventral temporal lobe structure such as the entorhinal cortices, Gloor (1997) has emphasized that auditory area 22, visual area 20, and the caudal third of the parietal region 7a, send major afferents to this region. These areas are either directly under or very proximal to the sensors (O2, T6, P4) from which we discerned the largest attenuation of power density for the qEEG and power density as inferred by LORETA when the wire mesh toque was being worn.

Although the measurement of any potential difference might be considered unlikely even with the appropriate referencing to an artery within the section, the EFA solution was distinctly acetic. Consequently there would be sufficient protons within the aqueous-ethanol environment that could have produced the potential difference assuming there was a disparity of charge. A disparity of charge usually requires some structural impedance that prevents homogenous distribution.

This intrinsic (micro) structure appeared to encourage a type of resonance with or the emission of frequencies within the theta and higher beta and gamma bands. According to empirical measurements (Tsang et al., 2004) the inductance per meter (permeability) of cortical grey matter at 1 kHz (the approximate duration average action potentials, i.e., 1 ms) is about 10^{-2} H. The permittivity for grey matter is $\sim 2 \cdot 10^{-1}$ Farads/m. Application of the classic formula for a circuit where resonance frequency is $f = 1/2(2\pi \cdot (LC)^{-1/2})$, L is inductance, and C is capacitance, the solution is about 7 Hz.

Although these measures are based upon fresh tissue within physiological level pH (in the order of 7.4–7.0), the calculated pH within 10 nm of cell membranes is more likely to be 2.5–3.0. This is within the range of the pH of the EFA solution in which the brain sections had been maintained and the present measures were collected. The average pH of EFA is about 3.45 which is similar to that when the sensor was immediately adjacent to the tissue surface. The study of simulated cortex by Rouleau and Persinger (2014) demonstrated the relevance of narrow-band pH as a potential regulator of human-coherent qEEG spectra.

Together, the data indicate that structural features which are preserved in fixed post-mortem tissue contribute to non-homogeneity of electric potential differences when referenced to a common point. Rostrocaudal and interhemispheric differences as a function of spectral power density revealed topographies which are perhaps intrinsic to the structure of the brain involved. The extent to which these findings are generalizable is unknown; however, the convergent findings presented here do suggest that some properties of living and non-living human brains overlap. The parahippocampal gyrus consistently demonstrated anomalies relative to structures within the same brain-space.

4. Materials & methods

4.1. Mitsar qEEG system, sLORETA, & WinEEG software

All qEEG measurements were completed with the use of a Mitsar qEEG system. For human participants, a 19-channel system was employed which was connected to a Lenovo ThinkPad laptop running Windows 7. The qEEG cap contained sensors positioned according to the 10–20 International System of Electrode Placement. A sodium-based electrogel was applied in order to establish cap-scalp and ear-sensor interfaces. For fixed tissue, needle-probes were inserted into the fixed brains directly. Electric potential differences were logged within WinEEG Version 2.93.59 (07.2013). Impedance values for all sensors were regulated to $< 5\ k\Omega$. A sampling rate of 250 Hz remained consistent across all experiments.

Spectral power densities were extracted in 30 s segments with 8 s epochs, and imported to SPSS v.20. For narrow-band investigation, raw data were extracted in 30 s segments from WinEEG as ASCII files, imported to SPSS v.20, standardized, and spectral analyzed. LORETA current spectral densities were obtained by first generating Talairach Electrode Coordinates which, when applied with the appropriate transformation matrix, allows the user to navigate voxels in 3D space and query the system for CSD values.

4.2. Copper screen-line toque & procedure

A black acrylic knit cap was retrofitted with a dual-layer of 28-gauge copper mesh wire lining (i.e. Copper Blocker). The mesh matrix consisted of evenly-distributed 5 mm squares that could expand by 1–2 mm in any direction, providing flexibility. The elasticity of the weave and mesh lining were such that head sizes up to 60 cm in circumference could be accommodated. An identical cap that was not retrofitted served as a control. Each individual was fitted with a qEEG electrode cap which rested beneath either the copper-lined or control cap. Participants were asked to sit quietly within the chamber and remain relaxed. Low-light levels were maintained throughout the experiment. Baseline qEEG data were collected with the participant's eyes open and closed. Subsequent to baseline recordings, the experimenter informed the participant that an adjustment to the equipment was necessary in order to continue the experiment. During said time, the cap was switched to either a copper-lined or control cap. All participants were exposed to both cap conditions which were counterbalanced to eliminate order-effects. The procedure was approved by Laurentian University's Research Ethics Board.

4.3. Needle-probe placement

The current methods specified for the measurement of voltage from fixed human brain tissue are similar to those employed by Saroka et al. (2015) in order to measure the electrical and spectral properties of tumors within mice. In their study, the reference consisted of the animal"s tail. In the current study, the reference consisted of vasculature.

For coronal sections of human brain tissue, needle-probes were placed within the following areas which were always recorded in both hemispheres and included adjacent white matter for cortical loci: anterior cingulate, posterior cingulate, genu of corpus callosum, septum pellucidum, gyrus rectus, orbital gyrus, septal nucleus, head of the caudate nucleus, claustrum, putamen, globus pallidus (I & II), anterior commissure, posterior commissure, fibers of the internal capsule, corona radiata, nucleus accumbens, olfactory tubercle, amygdala, superior frontal gyrus, middle frontal gyrus, inferior frontal gyrus, CA fields $(1-3)$, parahippocampal gyrus, insular gyrus, superior temporal gyrus, middle temporal gyrus, inferior temporal gyrus, pillars of fornix, medial geniculate nucleus, lateral geniculate nucleus, sublenticular component of the posterior arm of the internal capsule, transverse temporal gyrus, fusiform gyrus, crus of fornix, substantia nigra, crus cerebri, red nucleus, pulvinar, tail of caudate nucleus, superior parietal lobule, columns of fornix, hypothalamus, mamillothalamic tract, anterior nucleus of the thalamus, ventral anterior nucleus of the thalamus, body of fornix, extreme capsule, external capsule, alveus, supramarginal gyrus, optic chiasm, optic nerve, optic tract, periaqueductal grey, and the cerebral peduncle. Measurements were performed sequentially and were counterbalanced with respect to factors such as hemisphere and type of tissue.

The unsectioned brain was equipped with 14 sensors which recorded simultaneously. Probes were inserted into the orbiotofrontal (Fp1, Fp2), inferior frontal (F7, F8), parahippocampal (T3, T4), insular (C3, C4), supramarginal (T5, T6), superior parietal (P3, P4), and lateral occipital gyri (O1, O2). Placement of each needle probe was performed with reference to adjacent landmark structures. Orbitofrontal probes were placed within the center of the most rostral convexity of the orbital gyri which bordered the clearly defined orbital sulci. Inferior frontal probes were placed within the center of the pars triangularis bordered by the anterior ascending ramus (caudally) and anterior horizontal ramus (rostrally). Parahippocampal probes were placed within the parahippocampal gyrus at a midway point along the rostrocaudal axis

between the rhinal fissure and collateral sulcus. Insular probes were inserted into the anterior gyri breves. Supramarginal probes were placed within the caudal component of the supramarginal gyrus where the posterior ascending limb of the lateral fissure formed a rostral border. Superior parietal probes were inserted into the superior parietal lobule at the dorsal-most extent of this convexity and at a half-way point between the postcentral fissure and the parieto-occipital fissure along the rostrocaudal axis. Lateral occipital probes were inserted at a point between the lateral occipital sulcus and the occipital pole, ventral to the intraparietal fissure.

Acknowledgments

The authors would like to thank Dr. Kevin Saroka for his equipment and technical expertise.

References

Alonso, A., Klink, R., 1993. Differential electroresponsiveness of stellate and pyramidal-like cells of medial entorhinal cortex layer II. J. Neurophysiol. 70 (1), 128–143.
Bear, M.F., 1996. A synaptic basis for memory storage in the cerebral cortex. Proc. Natl. Acad. Sci. 93, 13453–13459.
Buzsáki, G., 2002. Theta oscillations in the hippocampus. Neuron 33 (3), 325–340.
Crick, F., Koch, C., 1990. Towards a neurobiological theory of consciousness. Semin. Neurosci. 2, 263–275.
Crick, F., Koch, C., 2003. A framework for consciousness. Nat. Neurosci. 6 (2), 119–126.
Dotta, B.T., Murugan, N.J., Karbowski, L.M., Lafrenie, R.M., Persinger, M.A., 2014. Shifting wavelengths of ultraweak photon emissions from dying melanoma cells: their chemical enhancement and blocking are predicted by Cosic's theory of resonant recognition model for macromolecules. Naturwissenschaften 101 (2), 87–94.
Good, C.D., Johnsrude, I., Ashburner, J., Henson, R.N., Friston, K.J., Frackowiak, R.S., 2001. Cerebral asymmetry and the effects of sex and handedness on brain structure: a voxel-based morphometric analysis of 465 normal adult human brains. Neuroimage 14 (3), 685–700.
Gloor, P., 1997. The Temporal Lobes and Limbic System. Oxford Press, Oxford.
Insausti, R., Juottonen, K., Soininen, H., Insausti, A.M., Partanen, K., Vainio, P., Pitkänen, A., 1998. MR volumetric analysis of the human entorhinal, perirhinal, and temporopolar cortices. Am. J. Neuroradiol. 19 (4), 659–671.
Joliot, M., Ribary, U., Llinas, R., 1994. Human oscillatory brain activity near 40 Hz coexists with cognitive temporal binding. Proc. Natl. Acad. Sci. 91 (24), 11748–11751.
Koenig, T., Prichep, L., Lehmann, D., Sosa, P.V., Braeker, E., Kleinlogel, H., John, E.R., 2002. Millisecond by millisecond, year by year: normative EEG microstates and developmental stages. Neuroimage 16 (1), 41–48.
Lehmann, D., 1990. Brain electric microstates and cognition: the atoms of thought. Machinery of the Mind. Birkhäuser Boston, pp. 209–224.
Llinas, R., Pare, D., 1991. Of dreams and wakefulness. Neuroscience 44, 521–535.
Llinas, R., Ribary, U., 1993. Coherent 40-Hz oscillation characterizes dream state in humans. Proc. Natl. Acad. Sci. 90, 2078–2081.
Meador, K.J., Ray, P.G., Echauz, J.R., Loring, D.W., Vachtsevanos, G.J., 2002. Gamma coherence and conscious perception. Neurology 59, 847–854.
Morgan, A.H., McDonald, P.J., Macdonald, H., 1971. Differences in bilateral alpha activity as a function of experimental task, with a note on lateral eye movements and hypnotizability. Neuropsychologia 9 (4), 459–469.
Nunez, P.L., 1995. Neocortical, Dynamics and Human EEG Rhythms. Oxford University Press., New York.
Persinger, M.A., Dotta, B.T., Karbowski, L.M., Murugan, N.J., 2015. Inverse relationship between photon flux densities and nanotesla magnetic fields over cell aggregates: quantitative evidence for energetic conservation. FEBS Open Bio.
Persinger, M.A., 1999. Is there more than one source for the temporal binding factor for human consciousness? Percept. Mot. Skills 89 (3f), 1259–1262.
Pruessner, J.C., Köhler, S., Crane, J., Pruessner, M., Lord, C., Byrne, A., Evans, A.C., 2002. Volumetry of temporopolar, perirhinal, entorhinal and parahippocampal cortex from high-resolution MR images: considering the variability of the collateral sulcus. Cereb. Cortex 12 (12), 1342–1353.
Raz, N., Gunning-Dixon, F., Head, D., Rodrigue, K.M., Williamson, A., Acker, J.D., 2004. Aging, sexual dimorphism, and hemispheric asymmetry of the cerebral cortex: replicability of regional differences in volume. Neurobiol. Aging 25 (3), 377–396.
Richards, P.M., Koren, S.A., Persinger, M.A., 1992. Experimental stimulation by burst-firing weak magnetic fields over the right temporal lobe may facilitate apprehension in women. Percept. Mot. Skills 75 (2), 667–670.
Rouleau, N., Persinger, M., 2014. Cerebral networks of interfacial water: analogues of the neural correlates of consciousness in a synthetic three-shell realistic head model. J. Signal Inf. Process. 5 (4), 143.
Saroka, K.S., Caswell, J.M., Lapointe, A., Persinger, M.A., 2014. Greater electroencephalographic coherence between left and right temporal lobe structures during increased geomagnetic activity. Neurosci. Lett. 560, 126–130.
Saroka, K.S., Karbowski, L.M., Murugan, N.J., Persinger, M.A., 2015. Evidence of “trapped” voltage spectrum residuals within mouse melanoma tumors for about 30 min following brief exposures to treatment-related, physiologically-patterned magnetic fields. Arch. Cancer Res. 3 (29), 1–5.
Saroka, K.S., Persinger, M.A., 2014. Quantitative evidence for direct effects between earth-ionosphere schumann resonances and human cerebral cortical activity. Int. Lett. Chem., Phys. Astron. 20.
Tsang, E.W., Koren, S.A., Persinger, M.A., 2004. Power increases within the gamma range over the frontal and occipital regions during acute exposures to cerebrally counterclockwise rotating magnetic fields with specific derivatives of change. Int. J. Neurosci. 114, 183–194.
Van Essen, D.C., Drury, H.A., 1997. Structural and functional analyses of human cerebral cortex using a surface-based atlas. J. Neurosci. 17 (18), 7079–7102.
Van Strien, N.M., Cappaert, N.L.M., Witter, M.P., 2009. The anatomy of memory: an interactive overview of the parahippocampal–hippocampal network. Nat. Rev. Neurosci. 10 (4), 272–282.
Watkins, K.E., Paus, T., Lerch, J.P., Zijdenbos, A., Collins, D.L., Neelin, P., Evans, A.C., 2001. Structural asymmetries in the human brain: a voxel-based statistical analysis of 142 MRI scans. Cereb. Cortex 11 (9), 868–877.
Witter, M.P., 1993. Organization of the entorhinal–hippocampal system: A review of current anatomical data. Hippocampus 3 (S1), 33–44.